Biosensors and Bioelectronics 31 (2012) 176–181

Contents lists available at SciVerse ScienceDirect

Biosensors and Bioelectronics

journal homepage: www.elsevier.com/locate/bios

Enzymatic glucose biosensor based on CeO_2 nanorods synthesized by non-isothermal precipitation

Dewyani Patil*, Nguyen Quoc Dung, Hyuck Jung, Se Yong Ahn, Dong Mi Jang, Dojin Kim*

Department of Materials Science and Engineering, Chungnam National University, Daejeon 305-764, Republic of Korea

ARTICLE INFO

Article history:
Received 15 September 2011
Accepted 8 October 2011
Available online 17 October 2011

Keywords:
Glucose biosensor
CeO_2 nanorods
GOx
Amperometric biosensor
EIS behavior

ABSTRACT

Cerium oxide nanorods (CeO_2 NRs) were synthesized without templates through a low cost and simple non-isothermal precipitation method. The structure and morphology of CeO_2 NRs were characterized by X-ray diffraction and transmission electron microscopy. The CeO_2 NRs films, deposited on indium tin oxide (ITO)-coated glass substrates through electrophoretic deposition, were used for the immobilization of glucose oxidase (GOx). Field emission scanning electron microscopy, Fourier transform infrared spectroscopy, cyclic voltammetry, and electrochemical impedance spectroscopy were used to characterize the CeO_2 NRs/ITO and GOx/CeO_2 NRs/ITO electrodes. The GOx/CeO_2 NRs/ITO electrode exhibits a linear range for the detection of glucose from 2 to 26 mM (correlation coefficient: 0.99) at 1–2 s response time. Biosensor sensitivity is 0.165 $\mu A\,mM^{-1}\,cm^{-2}$ with 100 μM detection limit. The anti-interference ability of the biosensor was also examined. The mediator-less application of CeO_2 NRs for glucose sensing was demonstrated.

1. Introduction

Biosensors such as glucose biosensors have received great attention owing to applications in clinical chemistry, biological, and chemical analyses, the food industry, and environmental monitoring. Several attempts have been made towards the fabrication of a biosensor for the estimation of glucose with glucose oxidase (GOx); most of these attempts use conducting polymers (Gvozdenovic et al., 2011; Patil et al., 2007) and semiconducting metal oxides (Chaniotakis and Sofikiti, 2008) to immobilize GOx. Recent studies reveal that the nanostructured metal oxides with reduced dimensionality (i.e., nanoparticles, nanorods, nanotubes, nanowires, and nanoribbons) have unique advantages in immobilizing enzymes and have high sensitivity due to high surface area, desirable microenvironment, and direct electron transfer between enzyme active sites and the electrode. Various nanostructured metal oxide materials (Liu, 2008; Ansary and Faddah, 2010) such as nanostructured ZnO in the form of nanorods (Asif et al., 2010), nanowires (Pradhan et al., 2010), nanotubes (Kong et al., 2009), nanocombs (Wang et al., 2006), nanofibers (Ahmad et al., 2010), CuO nanorods (Umar et al., 2009), TiO_2 nanotubes (Pang et al., 2009), and ZrO_2 nanoparticles (Yang et al., 2007) have been utilized for the fabrication of enzyme-based biosensors. However, glucose sensors based on nanostructured ZnO exhibit interference caused by uric and ascorbic acid (Zhai et al., 2010). ZrO_2 nanoparticle glucose biosensors use ferrocenium hexaflurophosphate as the electron transfer mediator (Yang et al., 2007), whereas TiO_2 nanotubes use covalent bonding to immobilize GOx (Zhang et al., 2011).

Nanostructured CeO_2 is one of the most promising materials for the fabrication of electrochemical biosensors due to interesting properties such as chemical inertness, nontoxicity, biocompatibility, high specific surface areas, electrical conductivity, and high electron transfer features. It has a wide band gap (3.4 eV) and a high isoelectric point (IEP) of about 9.2 (Ansari et al., 2008a,b), making it suitable for the adsorption of low IEP enzymes such as GOx (IEP4.2) (Yang et al., 2009) without the need for any harsh chemical treatment. Few reports deal with nanostructured CeO_2-based glucose biosensors. Ansari et al. reported a glucose sensor based on immobilized-GOx sol–gel derived from the nanostructured CeO_2/Au bioelectrode using a $Fe[(CN)_6]^{3-/4-}$ mediator with high sensitivity (0.00287 $\mu A\,mg\,dL^{-1}\,cm^{-2}$), linearity in the range of 50–400 mg/dL, high detection limit (12 μM), and stability for 12 weeks (Ansari et al., 2008a,b). Saha et al. recently reported the synthesis of nanoporous CeO_2 thin films on platinum-coated glass plates (i.e., nanoporous CeO_2/Pt) using pulsed-laser deposition and investigated their glucose sensing properties. The GOx-immobilized nanoporous CeO_2/Pt bioelectrode showed linearity in the range of 1.39–8.33 mM and a shelf life of 10 weeks (Saha et al., 2009).

The present study reports on glucose biosensors based on the adsorption of GOx onto CeO_2 NRs. The CeO_2 NRs were synthesized

* Corresponding authors. Tel.: +82 42 821 6639; fax: +82 42 823 7648.
E-mail addresses: pdewyani@yahoo.in (D. Patil), dojin@cnu.ac.kr (D. Kim).

0956-5663/$ – see front matter © 2011 Elsevier B.V. All rights reserved.
doi:10.1016/j.bios.2011.10.013

without templates through a low cost and simple non-isothermal precipitation method. The sensing performance of the fabricated mediator-less CeO_2 NRs glucose biosensors based on sensitivity, detection limit, a linear range of detection, response time, and anti-interference ability is presented and discussed.

2. Experimental

2.1. Materials and instruments

Analytical reagent grade chemicals and de-ionized water were used throughout the present study. GOx (EC1.1.3.4, from *Aspergillus niger*, 200 U/mg) and D-glucose were purchased from Sigma and cerium nitrate ($Ce(NO_3)_3{\cdot}6H_2O$) was procured from Aldrich. The other chemicals such as potassium dihydrogen orthophosphate (KH_2PO_4), dipotassium hydrogen orthophosphate (K_2HPO_4), sucrose, and urea were obtained from Daejung Reagents Chemicals, South Korea. Potassium hexacyanoferrate (III) ($Fe(CN)_6^{3-}$) and Ascorbic acid (AA) were obtained from Alfa Aesar and ammonia solution (28–30%) was procured from Samchun Chemicals, South Korea. All electrochemical experiments were carried out in a 0.1 M phosphate buffer solution (PBS) prepared from K_2HPO_4 (0.075 M) and KH_2PO_4 (0.025 M); pH was adjusted to 7.0. Indium tin oxide (ITO)-coated glass substrates (size: ~0.5 cm × 3.0 cm) were cut from an ITO-coated glass sheet (size: 30 cm × 40 cm, 1.1 mm thick, sheet resistance: ~6.5 Ω/□) was procured from Samsung corning Co. Ltd. Korea.

2.2. Synthesis of CeO_2 nanorods

CeO_2 NRs were synthesized without templates by non-isothermal precipitation using cerium nitrate and liquid ammonia as the starting materials (Chen and Chang, 2005). In a typical experiment, an aqueous solution of cerium nitrate (0.2 M) was prepared in deionized water and was stirred continuously using a magnetic stirrer for 1 h at 70 °C. The appropriate amount of ammonia (28–30%) was slowly added dropwise to the reaction mixture with continuous stirring. Immediately after the addition of ammonia to the mixture, the reaction started and a yellow-colored precipitate formed. After 5 min, the reaction mixture was transferred into another water bath cooled at 0 °C where the reaction continued for 24 h. The resulting precipitate was filtered, washed several times with de-ionized water and ethanol, and dried at 60 °C overnight.

2.3. Preparation of CeO_2 NRs/ITO electrodes by electrophoretic deposition

The synthesized CeO_2 NRs were used to prepare CeO_2 NRs/ITO electrodes through the electrophoretic (EPD) method (Fukada et al., 2004). The suspension for EPD was prepared by adding CeO_2 NRs (5 mg/ml) to a solution containing ethanol and 3% acetylacetone. The suspension was sonicated for 2 h to maintain good dispersion and suspension in the solution. For EPD, a platinum mesh and an ITO-coated glass substrate were used as the anode and cathode, respectively, with a 1.0 cm separation. Deposition was carried out by applying a 30 V DC voltage between the electrodes. The voltage was supplied by a Unicorn Programmable DC power supply for the duration of 3 min. After deposition, the films were dried at room temperature for 24 h followed by annealing at 300 °C for 3 h in air.

2.4. Immobilization of the GOx enzyme

To immobilize GOx into the CeO_2 NRs film, the GOx solution was prepared by dissolving 10 mg GOx in 1 ml phosphate buffer (0.1 M, pH 7.0). For enzyme immobilization, 20 μL of GOx was dropped onto the CeO_2 NRs/ITO electrodes and dried at room temperature. The GOx-immobilized CeO_2 NRs/ITO electrodes were stored at 4 °C in the dark when not in use.

2.5. Preparation of the glucose solution

A glucose stock solution (0.5 M) was prepared in a 0.1 M phosphate buffer solution (pH 7.0) then left at room temperature for about 24 h prior to use to ensure the presence of the β-D-glucose form.

2.6. Electrochemical measurements

Electrochemical measurements were carried out in the three-electrode setup with GOx/CeO_2 NRs/ITO as the working electrode, a platinum mesh as the counter electrode, and the Ag/AgCl electrode as the reference electrode. PBS (0.1 M, pH 7.0) was used as the electrolyte during electrochemical study. Amperometric and cyclic voltammetric measurements were carried out using Potentiostat/Galvanostat (EG and G, Princeton Research Model 263A, USA) controlled by the electrochemistry software Powersuite 2.55. Electrochemical impedance spectroscopy (EIS) measurements were carried out at the open circuit potential (OCP) in the frequency range from 0.1 Hz to 10 kHz with 0.3 V amplitude of the superimposed AC signal. The spectra were also recorded in PBS (0.1 M, pH 7.0) containing a 5 mM $Fe(CN)_6^{3-}$ solution. Analysis of the impedance spectra was done by fitting the experimental results to equivalent circuits using the Z-view software from Scribner Associates. The quality of fitting to the equivalent circuit was first evaluated using the χ^2-value (i.e., the sum of squares of the differences between theoretical and experimental points) and then by limiting relative error in the value of each element in the equivalent circuit to 5%. EIS measurements were performed using Autolab potentiostat (PGSTAT128N, Metrohm, U.S.A.).

2.7. Characterization techniques

The CeO_2 NRs were characterized by X-ray diffraction (XRD) and transmission electron microscopy (TEM). The XRD analysis was performed with a Bruker diffractometer (D8, Advance, Bruker AXS model) with CuK_α radiation (λ = 1.5406 nm) operating at 40 kV and 40 mA. TEM was used to determine the size and morphology of CeO_2 NRs with a JEOL (JEM ARM 200F, JEOL, Japan) microscope. The GOx-immobilized CeO_2 NRs film was characterized by field emission scanning electron microscopy (FESEM) and Fourier transform infrared spectroscopy (FTIR). The FESEM microscopy analysis was carried out with a JEOL (JSM-7000F, JEOL, and Japan) microscope at an acceleration voltage of 5 kV and a working distance of 8 mm. The FTIR spectroscopy analysis of the CeO_2 NRs film and the GOx-immobilized CeO_2 NRs film was performed with a Bio-Rad spectrometer (FTS-7, Bio-Rad Laboratories Inc., U.S.A.) by the conventional KBr method in the spectral range 4000–400 cm^{-1}.

3. Results and discussion

3.1. Characterization of CeO_2 NRs and CeO_2 NR/ITO, GOx/CeO_2 NR/ITO electrodes

The CeO_2 NRs characterized by XRD [Supporting information Fig. S1] showed cubic fluorite structure (JCPDS # 43-1002). The grain size (D) was calculated by Debye–Scherrer formula (Cullity and Stock, 1956):

$$D = \frac{0.94\lambda}{B\cos\ \theta} \quad (1)$$

where D is the average size of the crystallite, assuming that the grains are spherical, λ is the wavelength of X-ray radiation, B is

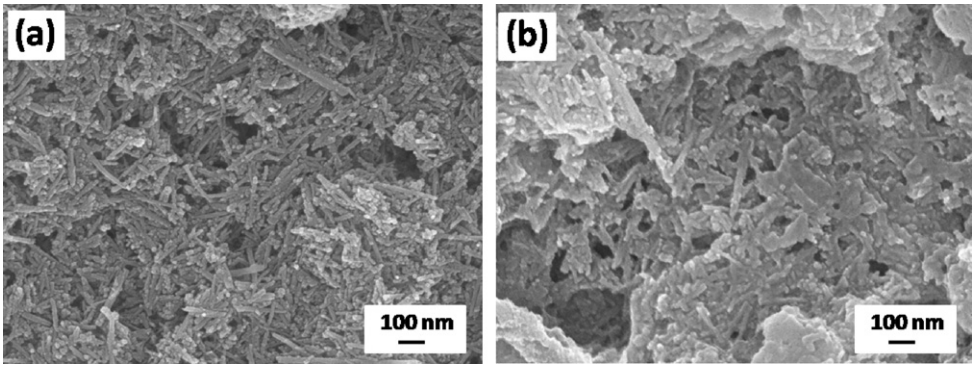

Fig. 1. FESEM images of (a) CeO_2 NRs/ITO and (b) GOx/CeO_2 NR/ITO electrodes.

the full width at half maxima of individual peak at 2θ (where θ is Bragg angle). The calculated grain size is found to be in the range of 3–5 nm. The TEM image of CeO_2 NRs [Inset of Fig. S1] exhibits a smooth and rod-like structure with the presence of some nanoparticles. The typical nanorods diameters are ~10 nm as evidenced by TEM.

The surface morphologies of the CeO_2 NRs/ITO and GOx/CeO_2 NRs/ITO electrodes characterized by FESEM are shown in Fig. 1. The FESEM image of the CeO_2 NR/ITO electrode [Fig. 1(a)] shows relatively uniform rod-like structures, whereas that of the GOx/CeO_2 NRs/ITO electrode [Fig. 1(b))] reveals that immobilized GOx does not affect the surface morphology of the CeO_2 NRs/ITO electrode. However, the FESEM image of GOx/CeO_2 NRs/ITO is a blurred image attributed to the nonconductive nature of GOx. This immobilization of GOx onto the CeO_2 NRs/ITO electrode was also confirmed by an FTIR spectroscopy analysis [see supplemental information Fig. S2].

3.2. Electrochemical studies

The cyclic voltammograms of the CeO_2 NRs/ITO and the GOx/CeO_2 NRs/ITO electrodes recorded in a 0.1 M PBS (pH 7.0) by cycling the electrode potential continuously between 0 and 0.8 V against Ag/AgCl at a potential scan rate of 0.02 V/s are shown in Fig. 2. The current density of the CeO_2 NRs/ITO electrode is higher than that of the bare ITO electrode (data not shown). The higher value of CeO_2 NRs/ITO electrode current density [Fig. 2(a)] may be attributed to the increased electroactive surface of the ITO electrode due to the deposition of CeO_2 NRs. This reveals that the CeO_2 NRs film facilitates electron transfer between the electrolyte medium and the electrode. After immobilization of GOx onto CeO_2 NRs/ITO, a significant decrease in the current density [Fig. 2(b)] was observed; this may be attributed to the insulating characteristics of GOx. Immobilized GOx in the electrode surface blocks the conducting sites of the CeO_2 NRs/ITO electrode. To confirm the adsorption of GOx, the cyclic voltammograms of GOx/CeO_2NRs/ITO were recorded in 0.1 M PBS (pH 7.0) with 2 mM glucose [Fig. 2(c)]. Comparing this with the measurements without glucose, shown in Fig. 2(b), shows an obvious increase in current density above the 0.45 V potential in the cyclic voltammogram recorded in the presence of 2 mM glucose.

The Nyquist impedance plot (Daniels and Pourmand, 2007) of the ITO electrode recorded in 0.1 M PBS (pH 7.0) containing 5 mM KF solution is shown in Fig. 3(a). It is modeled by an electrical equivalent circuit depicted in Fig. S3, consisting of electrolyte resistance (R_s), charge transfer resistance (R_{ct}), and double layer capacitance (C_{dl}). A constant phase element (CPE) is introduced into the circuit instead of a pure capacitor to give a more accurate fit. Fig. 3(b) shows the Nyquist impedance plot of the CeO_2 NRs/ITO electrode recorded in 0.1 M PBS (pH 7.0) containing 5 mM KF solution. The Randles circuit (Chen et al., 2008) depicted in the inset of Fig. 3 was used to model the impedance of the CeO_2 NRs/ITO electrode. It consists of R_s, R_{ct}, C_{dl}, and diffusion impedance (Z_w). In the Randles circuit, it is assumed that R_{ct} and Z_w are parallel to the interfacial double layer capacitance. Thus, the impedance plot of the CeO_2

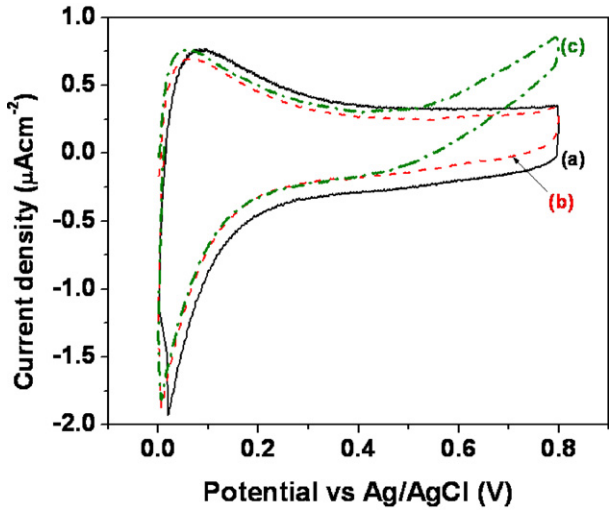

Fig. 2. Cyclic voltammograms of (a) CeO_2 NRs/ITO, (b) GOx/CeO_2 NR/ITO electrodes recorded in PBS (0.1 M, pH 7.0), and (c) GOx/CeO_2 NR/ITO electrode recorded in the presence of 2 mM glucose in PBS.

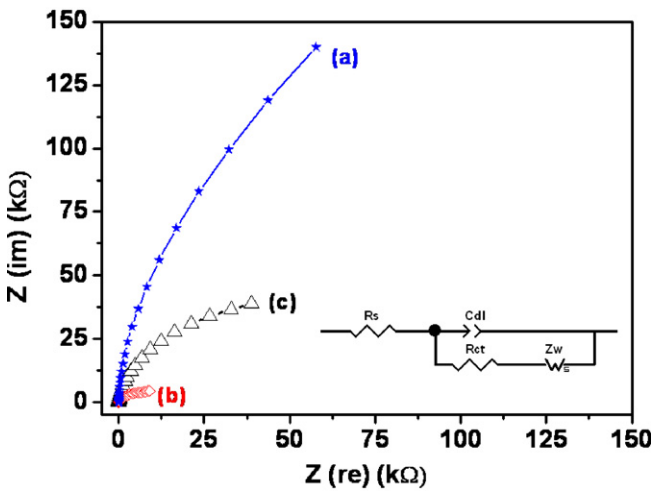

Fig. 3. Nyquist impedance plots for (a) ITO, (b) CeO_2 NRs/ITO, and (c) GOx/CeO_2 NR/ITO electrodes recorded in PBS (0.1 M, pH 7.0) containing 5 mM $Fe(CN)_6^{3-}$. Insets show the equivalent circuits used to model the impedance plots.

Table 1
Impedance parameter values extracted from the best fit to the equivalent circuit for impedance spectra recorded in PBS (0.1 M, pH 7.0) containing 5 mM KF.

Impedance parameter	ITO	CeO_2/ITO	GOx/CeO_2/ITO
R_s (Ω)	62.78	63.62	62.45
C_{dl} (F/m)	8.99×10^{-6}	1.58×10^{-5}	1.53×10^{-5}
n	0.9649	0.9381	0.9558
R_{ct} (Ω)	40.75×10^{4}	9.14×10^{2}	51.87×10^{3}
W (Ω)	–	17.46×10^{3}	44.26×10^{3}

NRs/ITO electrode [Fig. 3(b)] can be fitted with a semicircle at higher frequencies and with a line at the low frequency region. The semicircle is attributed to limited electron transfer and is characterized by R_{ct} and C_{dl}. The impedance parameter values of the best fit to the experimental impedance plots for the ITO and the CeO_2 NRs/ITO electrodes are given in Table 1. The R_{ct} value for CeO_2 NRs/ITO is approximately 914.4 Ω, about 315 times lower than that for ITO. The lower value of R_{ct} for CeO_2 NRs/ITO reveals that CeO_2 NRs provide an increased electroactive surface on the ITO electrode as well as enhanced electron transfer between electrode and medium. However, when GOx is immobilized onto the CeO_2 NRs/ITO electrode, R_{ct} of the GOx/CeO_2 NRs/ITO electrode [Fig. 3(c)] increases to 51.87 kΩ; this value is about 57 times greater than that of the CeO_2 NRs/ITO electrode. The higher R_{ct} value is attributed to the hindrance of electron transfer thereby indicating the immobilization of insulating GOx onto the CeO_2 NRs/ITO electrode. The EIS results reveal the immobilization GOx onto CeO_2 NRs/ITO; this is in agreement with the cyclic voltammetry study.

Zhai et al. reported electrochemical deposition of ZnO NR array on ITO for immobilization of GOx and performed the EIS studies of ZnO modified ITO electrodes synthesized at different conditions (Zhai et al., 2010). They have analysed the EIS spectra in terms of electron transfer resistance (R_{ct}), however the details of R_{ct} is not given. Fang et al. reported ZnO hollow nanospheres for GOx immobilization and performed EIS measurements of Nafon/GOx/ZnO-HNSPs/GCE (Fang et al., 2011). In the present study, the EIS spectra of ITO, CeO_2 NRs/ITO and GOx/CeO_2 NRs/ITO are explained with the help of equivalent circuit and its impedance parameters.

3.3. Amperometric response of the GOx/CeO_2 NR/ITO electrode

Hydrodynamic voltammogram [Inset of Fig. 4] for GOx/CeO_2 NRs/ITO electrode was obtained by applying different potential from 0.5 V to 0.9 V by step of 0.1 V versus Ag/AgCl to presence of 3 mM glucose in PBS (0.1 M, pH 7). There was no change in current after addition of 3 mM glucose at lower voltage than 0.5 V. The maximum change in current to addition of 3 mM glucose was observed at 0.8 V therefore, applied potential of 0.8 V was selected for further characterization of GOx/CeO_2 NRs/ITO electrode.

The steady state amperometric response of the GOx/ITO and GOx/CeO_2 NRs/ITO electrodes were recorded at the potential of 0.8 V (versus Ag/AgCl) in PBS (0.1 M, pH 7.0) for successive additions of glucose (at 1 mM and 2 mM/step) is shown in Fig. 4. The GOx/ITO electrode [Fig. 4(a)] shows the response to 1 mM glucose and there is no change in current density with further addition of glucose aliquots. The GOx/CeO_2 NRs/ITO electrode [Fig. 4(b)] shows a rapid response for each glucose addition, related to the immobilization of GOx onto the CeO_2 NRs/ITO electrode.

Amperometric response exhibits an increase upon addition of 1 mM glucose relevant to the background current; this increase is attributed to the good catalytic behavior of GOx/CeO_2 NRs than ITO. The GOx/CeO_2 NRs/ITO electrode achieved 90% steady state current within 1–2 s, indicating fast electron transfer between CeO_2 NRs and enzymatically generated H_2O_2. To explain the mechanism, the effect of oxygen on amperometric detection of glucose

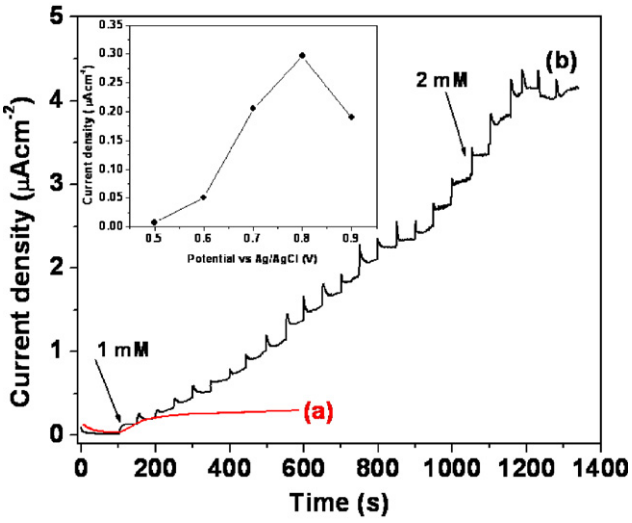

Fig. 4. Response of the (a) GOx/ITO and (b) GOx/CeO2 NR/ITO electrode at 0.8 V (against Ag/AgCl) to successive additions of glucose with 1 mM and 2 mM/step in PBS (0.1 M, pH 7.0). Inset shows hydrodynamic voltammogram of GOx/CeO2 NR/ITO electrode to 3 mM glucose in PBS.

in PBS was investigated and the corresponding result is presented in Fig. S5. The response current density to 1 mM glucose addition in absence and presence of oxygen is 0.125 μA cm^{-2} and 14.71 μA cm^{-2} respectively. In presence of oxygen the response current density was increased. It shows that the glucose sensing mechanism based on oxidation of glucose in presence of oxygen and enzymatically generated H_2O_2 detection (Wang et al., 2009). The reaction mechanism of glucose sensing by GOx/CeO_2 NRs/ITO electrode can be explained by the following reactions. The oxidation of glucose is explained by reaction (2) (Kong et al., 2009). The enzymatically generated H_2O_2 can decompose as shown in reaction (3) (Singh et al., 2011) and may react with CeO_2 as shown in reaction (4) and (5).

$$\text{Glucose} + O_2 \xrightarrow{\text{GOx}} \text{Glucanolactone} + H_2O_2 \quad (2)$$

$$H_2O_2 \rightarrow 2H^+ + O_2 + 2e^- \quad (3)$$

$$2CeO_2 + 2H^+ + 2e^- \rightarrow Ce_2O_2 + 2H_2O \quad (4)$$

$$2CeO_3 + H_2O \rightarrow 4Ce_2O_2 + 4e^- \quad (5)$$

A number of experiments were carried out to measure the steady state amperometric response of the GOx/CeO_2 NRs/ITO electrode to the addition of glucose in PBS (0.1 M, pH 7.0) solution. The standard error estimate in the response (measured for three electrodes) is ~1%, suggesting good tolerance as well as repeatability.

Steady state amperometric responses are used to construct the calibration curve of the GOx/CeO_2 NRs/ITO electrode; the corresponding calibration curve is presented in Fig. 5(a). The error bar indicates the standard error in the response measured for three different electrodes. The GOx/CeO_2 NRs/ITO electrode exhibits good linearity for sensing glucose from 2 to 26 mM with a correlation coefficient of 0.99. The sensitivity of GOx/CeO_2 NRs/ITO calculated from the slope of the calibration curve is 0.165 μA mM^{-1} cm^{-2}. The limit of detection of glucose is found to be 100 μM, at a signal to noise ratio of 3.

The apparent Michaelis–Menten constant (K_m) and the maximum response current density were calculated for immobilized GOx using the Linweaver–Burke plot as reported by Shu and Wilson (1976). The plot of reciprocal response current density against the reciprocal of glucose concentration is known as the Linweaver–Bruke plot obtained from the data presented in Fig. 5(a) for GOx/CeO_2 NRs/ITO shown in Fig. 5(b). The values of K_m and

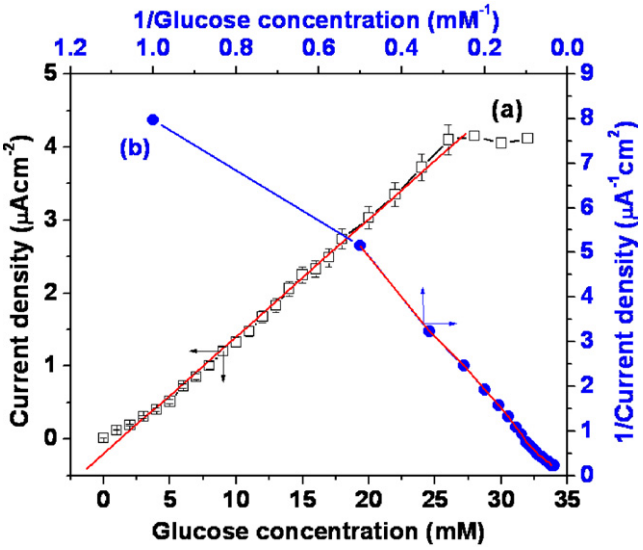

Fig. 5. (a) Calibration curve of the GOx/CeO_2 NR/ITO electrode and (b) Lineweaver–Burk plot for the GOx/CeO_2 NR/ITO electrode.

the maximum response current density are calculated from the intercept and the slope of this plot. The maximum response current density calculated for the GOx/CeO_2 NRs/ITO electrode is 4.16 μA cm^{-2} with K_m = 44.57 mM. The increased K_m value may be attributed to the porous structure of CeO_2 NRs/ITO. The GOx enzyme trapped into the pores of the CeO_2 NRs/ITO film increases mass transfer resistance, forming a barrier between GOx and glucose reaction.

The specificity of the GOx/CeO_2 NRs/ITO electrode was evaluated by measuring its The specificity of the GOx/CeO_2 NRs/ITO electrode was evaluated by measuring its response to successive addition of glucose in the presence of interfering species such as urea, sucrose and AA [see supplemental information Fig. S4]. The addition of 1 mM urea, sucrose and AA caused no observable interference on the response of GOx/CeO_2 NRs/ITO to glucose (1 mM). This observation is attributed to the selectivity of the glucose sensor fabricated with the GOx/CeO_2 NRs/ITO electrode.

Operational stability is related to the operating lifetime and reusability of the device; this is defined as the retention of activity of the enzyme when in use. The operational stability of the GOx/CeO_2 NR/ITO electrode was investigated in terms of the number of assays of 3 mM glucose and variation of the response current density while noting the number of reuses of the electrode assays. The response current density generated by 3 mM glucose remains fairly constant during 3 assays performed for the 3 days; thereafter, it slowly decreased.

The effect of temperature on the GOx/CeO_2 NR/ITO electrode response is investigated from 15 to 40 °C in the presence of 3 mM glucose in PBS (0.01 M, pH 7.0). The amperometric measurement at each temperature is recorded on a fresh electrode with a glucose concentration of 3 mM. The current response increases with temperature increase between 15 and 40 °C. Thereafter, current response decreases rapidly due to the denaturing of the enzyme. It is therefore strongly recommended to use the electrode between 15 and 25 °C to prolong sensor lifetime because the enzyme easily denaturizes at high temperature.

Only two reports exist on glucose biosensors based on sol–gel-derived nanostructured CeO_2 and pulsed-laser-deposited nanoporous CeO_2 films. Compared with these reports, the current CeO_2 NR-based biosensor exhibits better performance except the K_m value. The current K_m value is higher than the previously reported glucose biosensors based on sol–gel-derived nanostructured CeO_2 (13.55 μM) (Ansari et al., 2008a,b), nanoporous CeO_2 (1.01 mM) (Saha et al., 2009), ZnO:Co nanoclusters (21 mM) (Zhao et al., 2007), polypyrrole films (37.6 mM) (Yildiz et al., 2005), and nano-$CaCO_3$ (21.4 mM) (Sun et al., 2007). This higher value implies that GOx immobilized in the CeO_2 NRs/ITO film has lower affinity to glucose. However, the present biosensor is relatively better in terms of a wide linear range, short response time, reasonably good sensitivity, and good selectivity than previously reported glucose biosensors based on sol–gel-derived nanostructured CeO_2 (Ansari et al., 2008a,b), nanoporous CeO_2 (Saha et al., 2009), TiO_2/copolymer (Chen and Dong, 2003), and polypyrrole (Uang and Chuan, 2003). In addition, the non-isothermal method provides a low cost, simple, and efficient method to synthesize CeO_2 NRs for biosensor applications; providing an economic method for large-scale production.

4. Conclusions

CeO_2 NRs synthesized by simple non-isothermal precipitation. The glucose biosensor based on CeO_2 NRs and GOx exhibits a linear range for the detection of glucose from 2 to 26 mM, a reasonably good and reproducible sensitivity of 0.165 μA mM cm^{-2}, with a response time of 1–2 s, a 100 μM limit of detection, and the Michaelis–Menten constant of 44.57 mM. It also exhibits good anti-interference ability. The results of this study clearly indicate that the CeO_2 NR matrix synthesized by non-isothermal precipitation is a promising material for the fabrication of a mediator-less glucose biosensor which can applicable in glucose measurements of diabetics. Future work will be aimed to optimize the synthesis parameters of CeO_2 NRs for glucose measurement in real sample.

Acknowledgements

This research was supported by the National Research Laboratory and WCU (R32-20026) programs of the Ministry of Education, Science and Technology of Korea.

Appendix A. Supplementary data

Supplementary data associated with this article can be found, in the online version, at doi:10.1016/j.bios.2011.10.013.

References

Ahmad, M., Pan, C., Luo, Z., Zhu, J., 2010. J. Phys. Chem. C 114, 9308–9313.
Ansary, A.E., Faddah, L.M., 2010. Nanotech. Sci. Appl. 3, 65–76.
Asif, M.H., Usman Ali, S.M., Nur, O., Willander, M., Strålfors, Brännmark.C., Englund, P., Elinder, U.H., Danielsson, F., Biosens, B., 2010. Bioelectron 25, 2205–2211.
Ansari, A.A., Kaushik, A., Solanki, P.R., Malhotra, B.D., 2008a. Electrochem. Commun. 10, 1246–1249.
Ansari, A.A., Solanki, P.R., Malhotra, B.D., 2008b. Appl. Phys. Lett. 92, 263901.
Chaniotakis, N., Sofikiti, N., 2008. Anal. Chim. Acta 615, 1–9.
Chen, X., Wang, Y., Zhou, J., Yan, W., Li, X., Zhu, J., 2008. Anal. Chem. 80, 2133–2140.
Chen, H.I., Chang, H.Y., 2005. Solid State Commun. 133, 593–598.
Chen, X., Dong, S., 2003. Biosens. Bioelectron. 18, 999–1004.
Cullity, B.D., Stock, S.R., 1956. Elements of X-ray diffraction, 3rd ed., International edition Prentice Hall Co., USA.
Daniels, J.S., Pourmand, N., 2007. Electroanalysis 19, 1239–1257.
Fang, B., Zhang, C., Wang, G., Wang, M., Ji, Y., 2011. Sens. Actuators B: Chem., 040, doi:10.1016/j.snb.2010.12.
Fukada, Y., Nagarajan, N., Mekky, W., Bao, Y., Kim, H.S., Nicholson, P.S., 2004. J. Mater. Sci. 39, 787–801.
Gvozdenovic, M.M., Jugovic, B.Z., Bezbradica, D.I., Antov, M.G., Knez˘evic-Jugovic, Z.D., Grgur, B.N., 2011. Food Chem. 124, 396–400.
Kong, T., Chen, Y., Ye, Y., Zhang, K., Wang, X., 2009. Sens. Actuators B: Chem. 138, 344–350.
Liu, A., 2008. Biosens. Bioelectron. 24, 167–177.
Pradhan, D., Niroui, F., Leung, K.T., 2010. ACS Appl. Mater. Interfaces 2, 2409–2412.
Pang, X., He, D., Luo, S., Cai, Q., 2009. Sens. Actuators B: Chem. 137, 134–138.

Saha, S., Arya, S.K., Singh, S.P., Sreenivas, K., Malhotra, B.D., Gupta, V., 2009. Biosens. Bioelectron. 24, 2040–2045.
Patil, D.J., Gaikwad, A.B., Patil, P., 2007. J. Phys. D 40, 2555–2562.
Sun, Wei., Gao, R., Jiao, K., 2007. J. Phys. Chem. B 111, 4560–4567.
Shu, F.R., Wilson, G.S., 1976. Anal. Chem. 48, 1676–1679.
Singh, S., Dosani, T., Karakoti, A.S., Kmar, A., Seal, S., Self, T.S., 2011. Biomaterials 32, 6745–6753.
Umar, A., Rahman, M.M., Al-Hajry, A., Hahn, Y.B., 2009. Electrochem. Commun. 11, 278–281.
Uang, Y.M., Chuan, T., 2003. Biosens. Bioelectron. 19, 141–147.
Wang, J.X., Sun, X.W., Wei, A., Lei, Y., Cai, X.P., Li, C.M., Dong, Z.L., 2006. Appl. Phys. Lett. 88, 233106.
Wang, Y.T., Yu, L., Zhu, Z.Q., Zhang, J., Zhu, J.Z., Fan, C.H., 2009. Sens. Actuators B: Chem. 136, 332–337.
Yang, K., She, G.W., Wang, H., Ou, X.M., Zhang, X.H., Lee, C.S., Lee, S.T., 2009. J. Phys. Chem. C 113, 20169–20172.
Yang, X., Zhang, Q., Sun, Y., Liu, S., 2007. IEEE Sens. J. 7, 1735–1741.
Yildiz, H.B., Kiralp, S., Toppare, L., Yagci, Y., 2005. Int. J. Biol. Macromol. 37, 174–178.
Zhang, Z., Xie, Y., Liu, Z., Rong, F., Wang, Y., Fu, D., 2011. J. Electroanal. Chem., 241–247.
Zhai, Y., Zhai, S., Chen, G., Zhang, K., Yue, Q., Wang, L., Liu, J., Jia, J., 2010. J. Electroanal. Chem., doi:10.1016/j.jelechem.2010.11.020.
Zhao, Z.W., Chen, X.J., Tay, B.K., Chen, J.S., Han, Z.J., Khor, K.A., 2007. Biosens. Bioelectron. 23, 135–139.